B

DESIGN AND WINDTUNNEL TEST RESULTS OF A FLAPPED LAMINAR FLOW AIRFOIL FOR HIGH-PERFORMANCE SAILPLANE APPLICATIONS

ICAS-94-5.4.3

L.M.M. Boermans and A. van Garrel
Delft University of Technology
Faculty of Aerospace Engineering
The Netherlands

Abstract

A laminar flow airfoil with camber changing flap, named DU89-134/14, has been designed and windtunnel tested for application in the high-performance sailplanes ASH-26E and ASW-27 produced by Alexander Schleicher Segelflugzeugbau, Germany. The ASH-26E is an 18m span selflaunching sailplane with retractable propellor and the ASW-27 is a 15m span FAI competition sailplane.
Primary objectives were: low drag at a specified range of lift coefficients and Reynolds numbers, no abrupt loss of lift beyond the upper boundary of the low drag bucket at high lift conditions - to avoid bad handling and climbing qualities in thermal flight conditions -, gradual stalling characteristics, and a maximum lift coefficient insensitive to leading edge contamination.
These requirements have been met, as verified experimentally, by the design of long laminar flow regions on the upper and lower surface and, at increasing angle of attack, a controlled growth of the turbulent separated area while transition moves forward to the leading edge. Flap deflections and artificial transition were integrated from the start into the design. Flexible slot sealings save drag and, at the high speed flap settings, the sealing on the lower surface enables the boundary layer to remain laminar up to 95 % chord, where pneumatic turbulators cause transition.
In comparison with the well-known Wortmann sailplane airfoil FX62-K-131/17, the new airfoil shows superior performance.

Introduction

At the Low Speed Windtunnel Laboratory of Delft University of Technology, Faculty of Aerospace Engineering, airfoil DU89-134/14 has been designed and windtunnel tested for application in the ASH-26E and ASW-27 high performance sailplanes, Fig. 1 and 2, produced by Alexander Schleicher Segelflugzeugbau, Germany.
The ASH-26E is an 18m span selflaunching sailplane with 50 hp Mid-West AE50R rotary engine and retractable propellor, and the ASW-27 is a 15m span FAI competition sailplane.

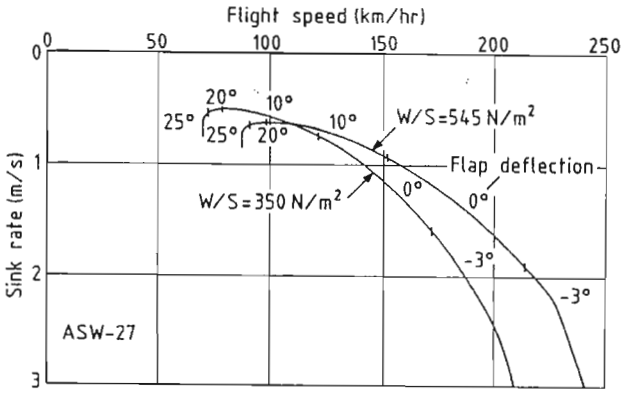

Fig. 3: Calculated performance of the ASW-27

A camber changing flap along the entire span of the wings is deflected at such an angle that the wing profile drag is minimum at the selected flight speed, as illustrated in the calculated speed polars of the ASW-27, Fig. 3. The sailplanes climb in thermals at high lift coefficients, i.e. low flight speeds, with a flap setting of 20° or 25° and fly in between the thermals with higher flight speeds and lower flap settings, frequently zero degrees.

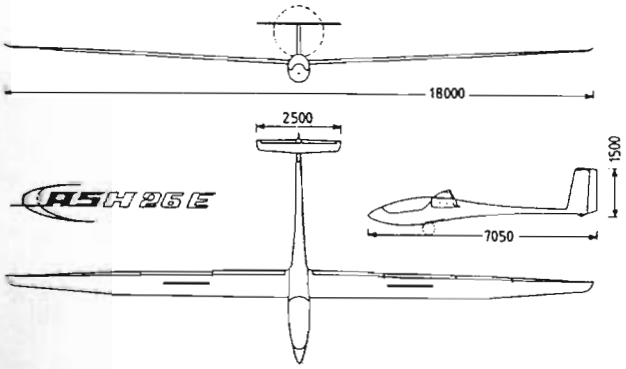

Fig. 1: Three-view drawing of the ASH-26E

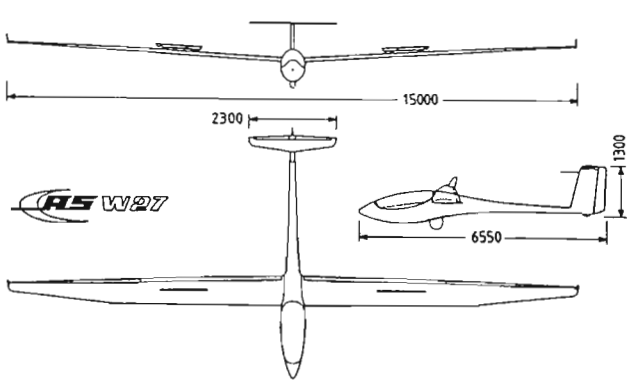

Fig. 2: Three-view drawing of the ASW-27

In a soaring contest the object is to realize the highest possible cross-country speed. Instruments, based on soaring flight optimization theory, enable the pilot to fly with optimum inter-thermal flight speeds, provided that the rate of climb in the next thermal, which has to be estimated in advance, is realized. In general, the better the rate of climb, the higher is the optimum inter-thermal flight speed and consequently the cross-country speed.

Modern sailplanes are capable to carry a relatively large amount of waterbalast in their wings. For instance, the wing loading of the ASW-27 can be increased by about 55 %, Fig. 3. This enables the pilot to realize higher cross-country speeds at strong thermal conditions since the improvement of the speed polar at inter-thermal flight speeds more than outweighs the lower climb rates - due to higher sink rate - in the thermals. At weak thermal conditions the opposite is true, and water will be dumped when thermal conditions deteriorate.

All in all, airfoils for high performance sailplane application have to be optimized for low drag at all practical flight speeds (multipoint design). In practice, the lift coefficient at low drag varies from about 0.25 to 1.5 and the Reynolds number from about $0.7*10^6$ to $3*10^6$.

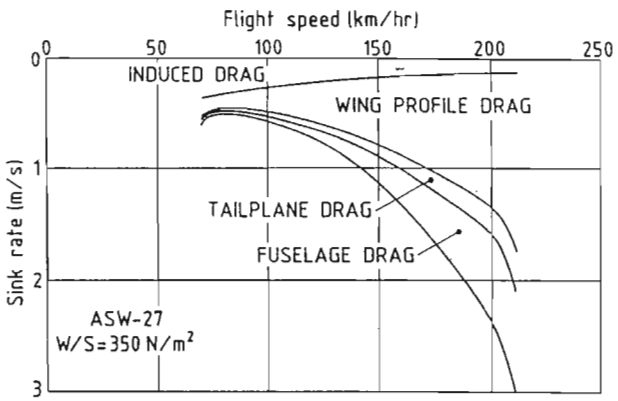

Fig. 4: Analysis of ASW-27 performance polar

Fig. 4 shows the calculated contribution of the wing, fuselage and tailplanes to the total drag and hence the rate of sink of the ASW-27. Typically, the wing contribution varies between 90% at low flight speed and 65% at high flight speed. The profile drag, which is relevant for the present paper, contributes from 25% at low flight speed up to 55% at high flight speed. Hence, a reduction in profile drag most effectively reduces the rate of sink at high flight speeds.

At the Low Speed Windtunnel Laboratory experience has been gained in designing and windtunnel testing of airfoils for sailplane application[1,2,3]. The next chapters describe the objectives, design and windtunnel tests of airfoil DU89-134/14 (Delft University, 1989, thickness 13.4%, camber changing flap 14% chord).

Design

The primary objectives of the airfoil design with camber changing flap were:

- low profile drag at lift coefficients between 0.25 and 1.5, and Reynolds numbers between $0.7*10^6$ and $3*10^6$,
- no abrupt decrease of lift (and increase of drag) beyond the upper boundary of the low drag bucket at high lift conditions,
- gradual stalling characteristics,
- maximum lift coefficient insensitive to leading edge contamination.

Given these requirements, the new airfoil was designed with the airfoil analysis and design code developed at the Low Speed Windtunnel Laboratory[4].

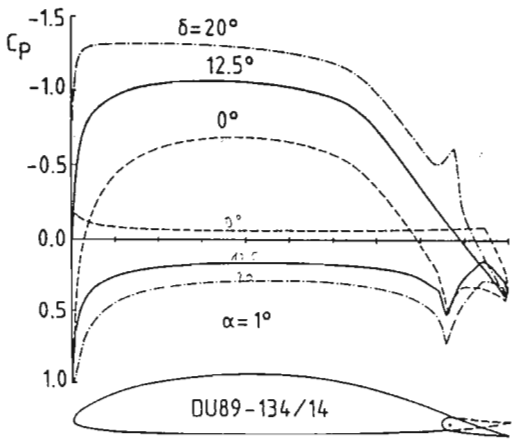

Fig. 5: Potential flow pressure distributions

Low drag at the intended lift coefficients and Reynolds numbers was achieved by the design of long laminar flow regions on the upper and lower surface in combination with a small flap, as indicated by the potential flow pressure distributions in Fig. 5. The pressure distributions at 0° and 20° flap deflection are representative for high and low flight speed respectively.

To save drag it is common practice to seal the upper and lower surface flap gaps with flexible mylar strips glued flush with the forward part of the airfoil and sliding on the flap. Such a sealing, in combination with the pressure distribution shown in Fig. 5 for the lower surface at zero flap deflection, enable the boundary layer to remain laminar beyond the flap hinge at high flight speeds.
Since the Reynolds number for transition on a flat plate is about $5*10^6$ at free flight conditions[5] and sailplane chord Reynolds numbers are $3*10^6$ at most, there is ample reserve for the boundary layer to remain laminar up to the trailing edge if the pressure distribution has a zero or favourable gradient. However, at low lift

coefficients the pressure level on the lower surface necessitates a pressure recovery to the trailing edge, as shown in Fig. 5. Calculations show that a turbulent boundary layer starting at the leading edge is able to reach the trailing edge without separation if the adverse pressure gradient starts at 95% chord utmost. A laminar boundary layer, however, will separate at this position and a detrimental laminar separation bubble, possibly reaching beyond the trailing edge, will appear. Hence, artificial transition control has to be applied. For that purpose several transition devices are applied in practice, such as tape with bulges, zig-zag tape or pneumatic turbulators[6]. The latter device, blowing a small amount of air through orifices periodically spaced in spanwise direction, is particularly suitable for the present purpose because of its negligible device drag (in the order of $5*10^{-6}$) at downward flap deflections, when the boundary layer on the flap lower surface is turbulent. The hollow flap serves as the duct for the air supply to the blowing orifices, and the air enters the flap via a small nozzle.

At positive flap deflections, the pressures induced by the corner at the hing position cause a laminar separation bubble. Extensive tests to eliminate this bubble on a previous airfoil, using mechanical and pneumatic turbulators, did not yield a drag decrease[4]. Probably the additional pressures due to the bubble, acting on the corner, have no component in flow direction and hence no additional pressure drag exists.

While the lower surface is squeezed out for low drag at high flight speeds and zero flap setting, the upper surface is tailored for low flight speeds at 20° flap deflection as well. In addition to transition, laminar and turbulent separation have to be controlled on the upper surface in order to realize the objectives mentioned before. Low drag was achieved by a long laminar flow extent, now followed by a so-called instability region[7], being a region with a slightly adverse pressure gradient to destabilize the laminar boundary layer, thus avoiding the formation of a detrimental laminar separation bubble.

The second requirement, to avoid an abrupt decrease of lift and accompanying increase of drag beyond the low drag bucket, was set to overcome the unfavourable handling and climbing qualities experienced with some high performance sailplanes; in thermal flight conditions the angle of attack varies and excursions beyond the low drag bucket are easily made. This goal was attained by a controlled growth of the turbulent separated area while transition moves gradually forward at increasing angle of attack; the loss of lift due to separation is compensated by the increase of lift on the forward part of the airfoil. This requirement, however, sets a limit to the extent of the laminar flow due to the pressure gradient in the turbulent pressure recovery region and the height of the pressure peak at the flap hinge position. A lower pressure peak is obtained by a reduction of the kink in the airfoil contour which in turn leads to a thinner flap. On the other hand, at zero flap deflection, the change in pressure distribution due to the corner at the hinge position (depression) may cause earlier transition and turbulent separation in the corner, and consequently higher drag at high speeds. Fig. 5 shows the final result of the optimization: a smooth upper surface pressure distribution and shape is present at 12.5 degrees flap deflection and laminar flow is expected up to about 65% chord at all flap deflections.

The third and fourth requirement are set by safety considerations relating to stalling behaviour and landing speed. Gradual stalling characteristics are obtained by a steady increase of the turbulent separated area with angle of attack (again) and the avoidance of bubble bursting at the leading edge (leading edge stall). The fourth requirement, stating that the maximum lift coefficient and hence the stall speed should not be sensitive to leading edge contamination (insect remains etc.), implies that the maximum lift coefficient of the airfoil does not depend on the achievement of laminar flow[1].

Windtunnel tests

Windtunnel, model, instrumentation, data reduction

The airfoil was tested in the Low Speed, Low Turbulence Windtunnel of Delft University of Technology, Faculty of Aerospace Engineering. The tunnel is of the closed return type and has a contraction ratio of 17.9. The interchangeable octagonal test section is 1.80 m wide and 1.25 m high. The turbulence level in the test section varies from 0.018% at 10 m/s to .07 % at 75 m/s.

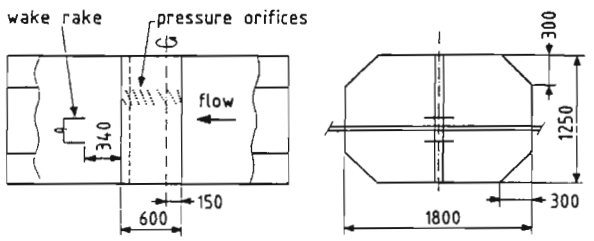

Fig. 6: Windtunnel model in test section

The windtunnel model had a chord of 0.60 m and a span of 1.25 m. It was installed vertically, Fig. 6, between mechanically actuated turntables which are flush with the test section top and bottom wall. A total of 91 orifices, 0.4 mm in diameter, were installed in 8 obligue rows to measure the airfoil pressure distribution.
Pneumatic turbulators were applied at the flap lower surface. The blowing air was supplied by pressuring the flap, and the total air volume flow as well as the internal pressure in the flap were measured.
Both on the upper and lower surface a flexible flap sealing was glued flush with the forward part of the airfoil, sliding over the flap surface.
A wake rake, mounted on a cross beam, and positioned 57% chord length behind the trailing edge, was set in the middle of the wake at each measurement. The wake rake employed 50 total-pressure tubes and 12 static-pressure tubes, all 1.5 mm in diameter.

All pressures were recorded by an automatically reading multi-tube liquid manometer (200 tubes) with a resolution of 1 Pa. The data were online reduced, and surface and wake pressure distributions as well as aerodynamic characteristics were presented on screen.

The model was tested at Reynolds numbers from 0.7 * 10^6 to 3 * 10^6, angles of attack from -13° to 20° and flap deflections from -20° to 50°.
The static pressure measurements at the model surface were reduced to standard pressure coefficients and numerically integrated to obtain section normal force and pitching moment coefficients. Profile drag coefficients were computed from the wake rake total and static pressures by the method of Jones[8].
Section lift coefficients were calculated from the normal force and profile drag coefficients.
Standard low speed wind tunnel boundary corrections[9], composed of solid and wake blockage, lift interference and wake buoyancy were applied to the section characteristics and pressure distributions.

Test results

The measured pressure distributions for α = 1° with flap deflection 0°, 12.5° and 20° at Reynolds number 2.5 * 10^6, 1.5 * 10^6 and 1.0 * 10^6 respectively are shown in Fig. 7. Tests at zero flap deflection with pneumatic turbulators at 95% and 93% chord on the lower flap surface revealed that 0.6 mm holes drilled at 93% chord with 8 mm interspace and a blowing rate of about 2 cm^3/sec per pneumatic turbulator yielded minimum drag. The blowing rate needed to obtain minimum drag is not critical, the curves show a flat optimum.

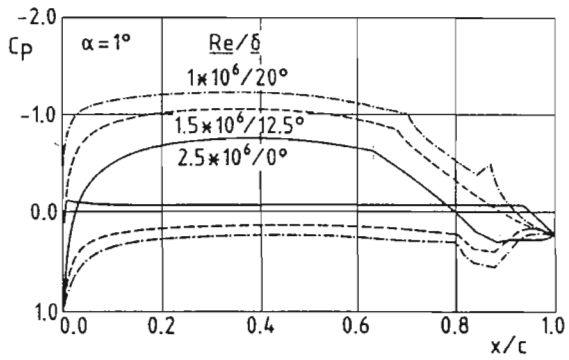

Fig. 7: Measured pressure distributions

In case of no blowing, there is a laminar separation bubble extending beyond the trailing edge and a clear whistling sound is heard which, according to stethoscope measurements, originates at the trailing edge and persists in a thin layer in the wake downstream. The sound disappears when blowing is activated. Drag increase due to blowing in the turbulent boundary layer at positive flap deflections could not be detected. Hence, there is no need to shut-off blowing.

As shown in Fig. 7 the pressure distributions on the upper surface indicate laminar flow followed by free transition at about 65% chord at 0° flap deflection, a smooth turbulent boundary layer pressure recovery at 12.5° flap deflection, and a laminar separation bubble type transition at 70% chord at 20° flap deflection. It is noted that the depression kink in the upper and lower surface pressure distribution at the hinge position could not be measured in more detail because the pressure orifices on the flap were covered by the flexible sealing.

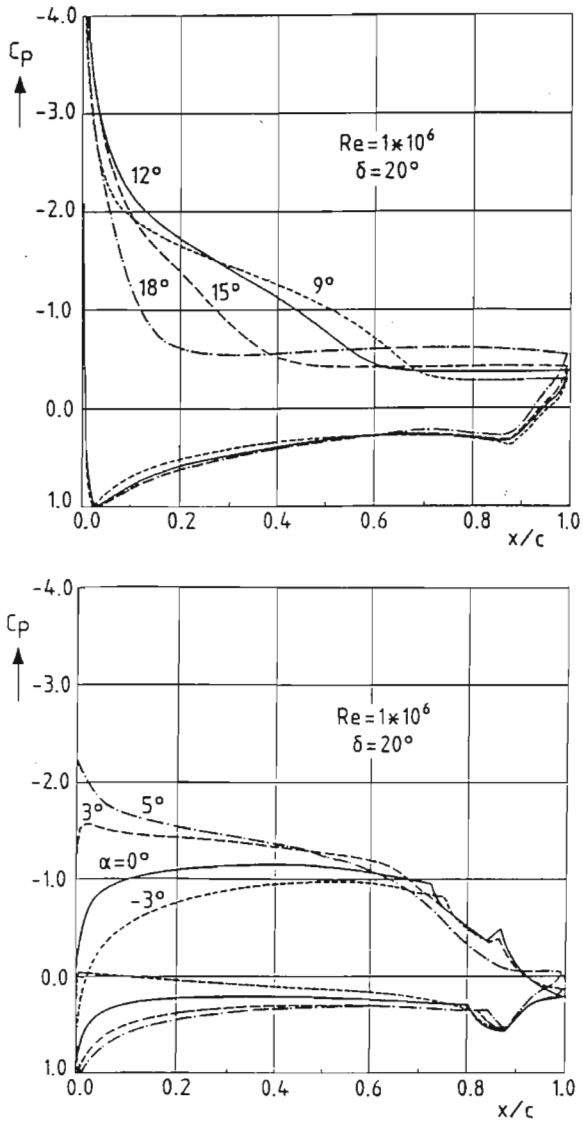

Fig. 8: Measured pressure distributions

Fig. 8 shows the pressure distributions for various angles of attack with a flap deflection of 20° at a Reynolds number of 1 * 10^6. At α = -3°, which is near the lower boundary of the low drag bucket, transition on the lower surface is on the verge of moving forward at decreasing angle of attack. At increasing angle of attack there is a laminar separation bubble on the lower surface which increases in length, eventually covering the corner at the hinge position.
On the upper surface there is a laminar separation bubble which disappears at α = 3°, being the upper boundary of the low drag bucket. As the angle of attack is increased further, transition moves gradually forward as

the suction peak at the nose develops, and turbulent boundary layer separation, starting at the trailing edge, moves forward slowly. The loss of lift due to separation is more or less compensated by the gain in lift of the attached flow surface.

At $\alpha = 12^{o}$, which corresponds to the maximum lift coefficient, transition is on the leading edge and turbulent separation occurs at about 60% chord. As the angle of attack is increased even further, the leading-edge suction peak does not collapse, indicating that leading edge stall does not occur, and turbulent separation moves forward to 20% chord at $\alpha = 18^{o}$. Hence, maximum lift does not depend on the achievement of laminar flow (contaminated leading edge) and stall is of the trailing edge type.

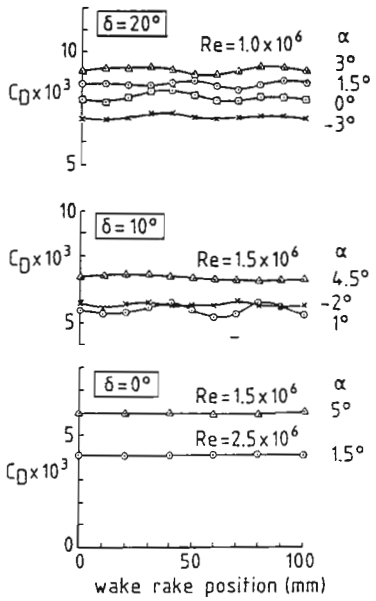

Fig. 9: Spanwise drag traverse measurements

Generally, at each flap deflection, spanwise wake traverse measurements were performed at several angles of attack, usually within the low drag bucket and at its boundaries, in order to check the two-dimensionality of the flow and to select a wake rake span position where the drag represents a mean value, to be used for the determination of the aerodynamic characteristics. Fig. 9 shows some typical results. At 10^{o} and 20^{o} flap deflection, the drag distribution shows a wavy character due to the presence of a laminar separation bubble on the upper and/or lower surface[10]. No bubbles are present at zero flap deflection, and the drag is constant along the span.

A selection of the two-dimensional aerodynamic characteristics measured at practical Reynolds numbers is presented in Fig. 10. Attention was paid to detect any hysteresis and to check reproduction by measuring at increasing and decreasing angle of attack; no hysteresis could be detected and reproduction was splendid.

The characteristics show that the primary objectives of low drag at lift coefficients between 0.25 and 1.5 and corresponding Reynolds numbers of 3 * 10^{6} and 0.7 * 10^{6}, no sudden decrease of lift beyond the upper

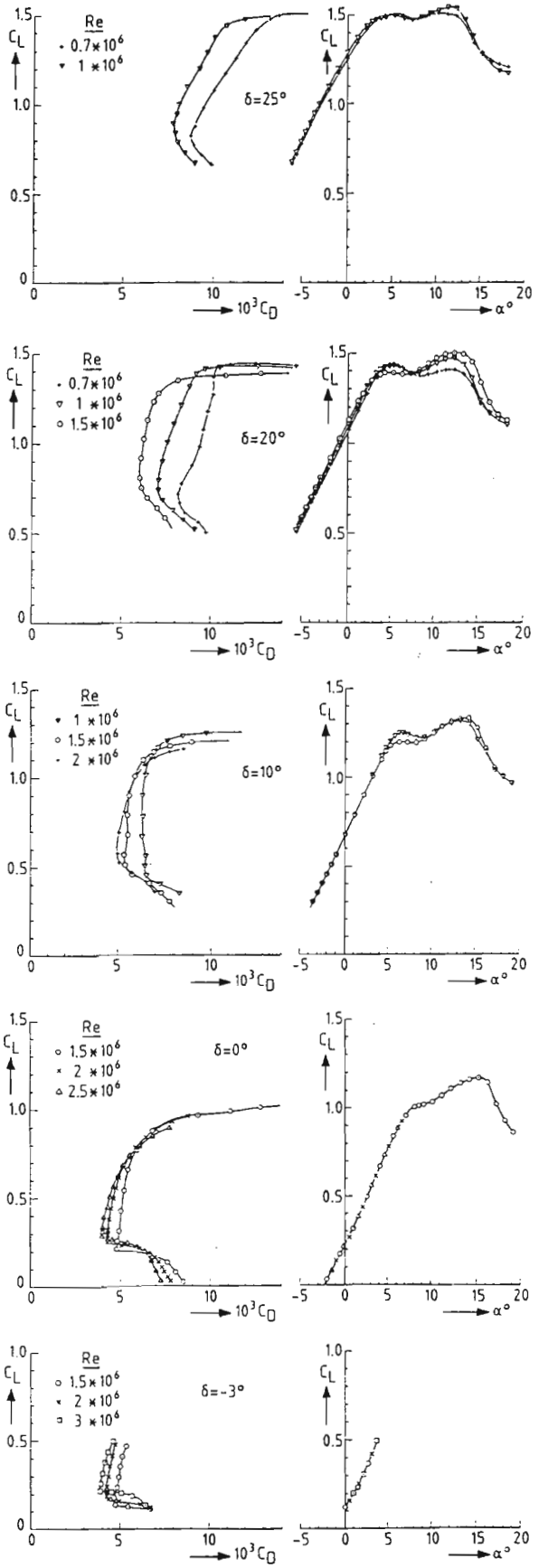

Fig. 10: Two-dimensional aerodynamic characteristics of airfoil DU-89-134/14

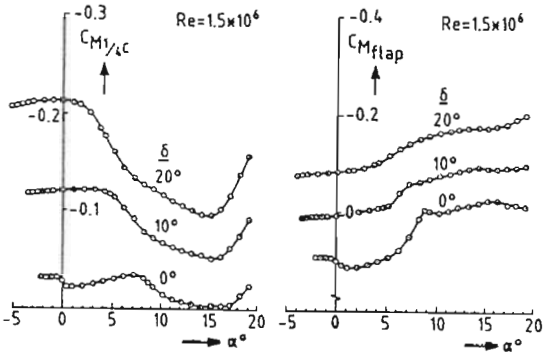

Fig. 10: Continued

boundary of the low drag bucket at high lift conditions (20° and 25° flap deflection) and gradual stalling characteristics, have been achieved.
The slight dent in the drag curve at 20° flap deflection and Reynolds number 0.7 * 10^6 is due to the laminar separation bubble on the upper surface. An attempt to eliminate the bubble by applying a 0.3 mm thick zig-zag tape turbulator at 63% chord and 65% chord yielded drag increase due to earlier separation of the turbulent boundary layer near the trailing edge. Calculation showed the same result, indicating that bubble type transition is preferable in this case.

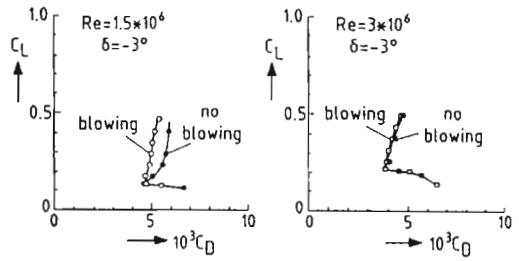

Fig. 11: Drag polars with and without blowing

Fig. 11 shows results of tests with and without pneumatic turbulators at -3° flap deflection. Due to this flap deflection there is a slight adverse pressure gradient behind the hinge position on the flap lower surface, which promotes transition. While elimination of the laminar separation bubble is still beneficial at Re = 1.5 * 10^6, blowing has little effect at Re = 3 * 10^6, indicating that free and forced transition nearly coincide. This result illustrates the stability of the laminar boundary, mentioned before, and the reserve with respect to the zero flap setting.

Concluding remarks

A flapped laminar flow airfoil, DU89-134/14, for the high performance sailplanes ASH-26E and ASW-27, has been designed theoretically and verified experimentally in the Low-Speed, Low-Turbulence Windtunnel of Delft University of Technology, Faculty of Aerospace Engineering.

The primary objectives of low profile drag at a specified range of lift coefficients and Reynolds numbers, no abrupt decrease of lift beyond the upper boundary of the low drag bucket at high lift conditions, gradual stalling characteristics and a maximum lift coefficient insensitive to leading edge contamination, have been achieved.

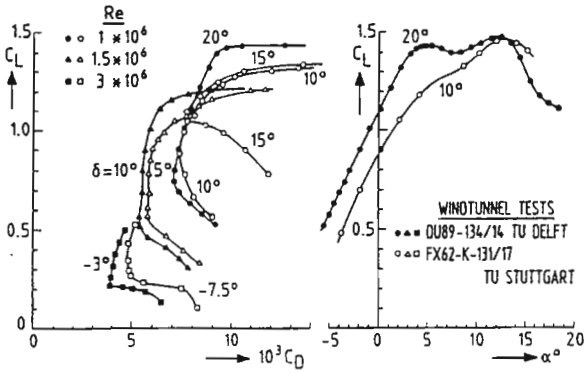

Fig. 12: Comparison of airfoil characteristics

Fig. 12 shows some typical characteristics of DU89-134/14 in comparison with the well-known Wortmann sailplane airfoil FX62-K-131/17[10] which was applied in the wing of the predecessor of the ASW-27, being the ASW-20. Note the different definition of the flap angle. The new airfoil has a wider overall low drag bucket, a 20% lower minimum drag coefficient, and similar gradual stalling characteristics.

First flight of the ASH-26E was on June 6th 1993, and first flight of the ASW-27 is expected autumn 1994. Performance of the ASH-26E has not been measured yet. However, comparison flights with modern sailplanes of comparable span show clear improvement in straight glide. Climbing performance is impressive, being closer to 25 m span Open Class sailplanes. Stall behaviour is very gentle, with full roll control, and wing drop does not occur. Test flights at zero flap deflection without turbulators reproduced the whistling sound which was heard in the windtunnel, proving that the flexible sealing is adequate and laminar flow is maintained on the lower flap surface.

Acknowledgements

The authors are greatly indebted to the sailplane designers M. Heide (ASH-26E) and G. Waibel (ASW-27) of Alexander Schleicher Segelflugzeugbau, Germany, for the valuable discussions on airfoil performance in relation to flight experience. Mr. Waibel's supposition that the laminar boundary layer would not be tripped by the flap sealing, was incentive and appeared to be true. The authors gratefully acknowledge the assistance of J. Bosschers during the windtunnel tests.

References

1. Boermans, L.M.M., Selen, H.J.W.: Design and tests of airfoils for sailplanes with an application to the ASW-19B. ICAS-paper 82-5.5.2, 1982.

2. Boermans, L.M.M., Waibel, G.: Aerodynamic and structural design of the Standard Class Sailplane ASW-24. ICAS-paper 88-2.7.7, 1988.

3. Boermans, L.M.M., Bennis, F.: Design and windtunnel tests of an airfoil for the horizontal tailplane of a Standard Class sailplane. Technical Soaring, Vol.16, No. 2, 1992.

4. Ingen, J.L. van, Boermans, L.M.M.: Aerodynamics at low Reynolds numbers: A review of theoretical and experimental research at Delft University of Technology, Proc. of Int. Conf. on Aerodynamics at Low Reynolds Numbers, paper 1, R.A.E.S., London, 1986.

5. Wells, C.S.: Effects of free stream turbulence on boundary layer transition. AIAA Journal, Vol. 5, No. 1, pp. 172-174, 1967.

6. Horstmann, K.H., Quast, A., Boermans, L.M.M.: Pneumatic turbulators - a device for drag reduction at Reynolds numbers below 5 * 10^6. AGARD CP-365, paper 20, 1984.

7. Wortmann, F.X.: Progress in the design of low drag airfoils. Boundary layer and flow control, Vol. 2. G.V. Lachmann, ed., Pergamon Press, 1961, pp. 748-770.

8. Jones, B.M.: Measurement of profile drag by the pitot-traverse method. R&M no. 1688, Brit. A.R.C., 1936.

9. Allen, H.J., Vincenti, W.G.: Wall interference in a two-dimensional flow windtunnel with consideration of the effect of compressibility. NACA Report 782, 1944.

10. Althaus, D.: Drag measurements on airfoil. OSTIV Publication 16, 1981.

11. Althaus, D.: Stuttgarter Profilkatalog I. Institut für Aero- und Gasdynamik der Universität Stuttgart, 1972.

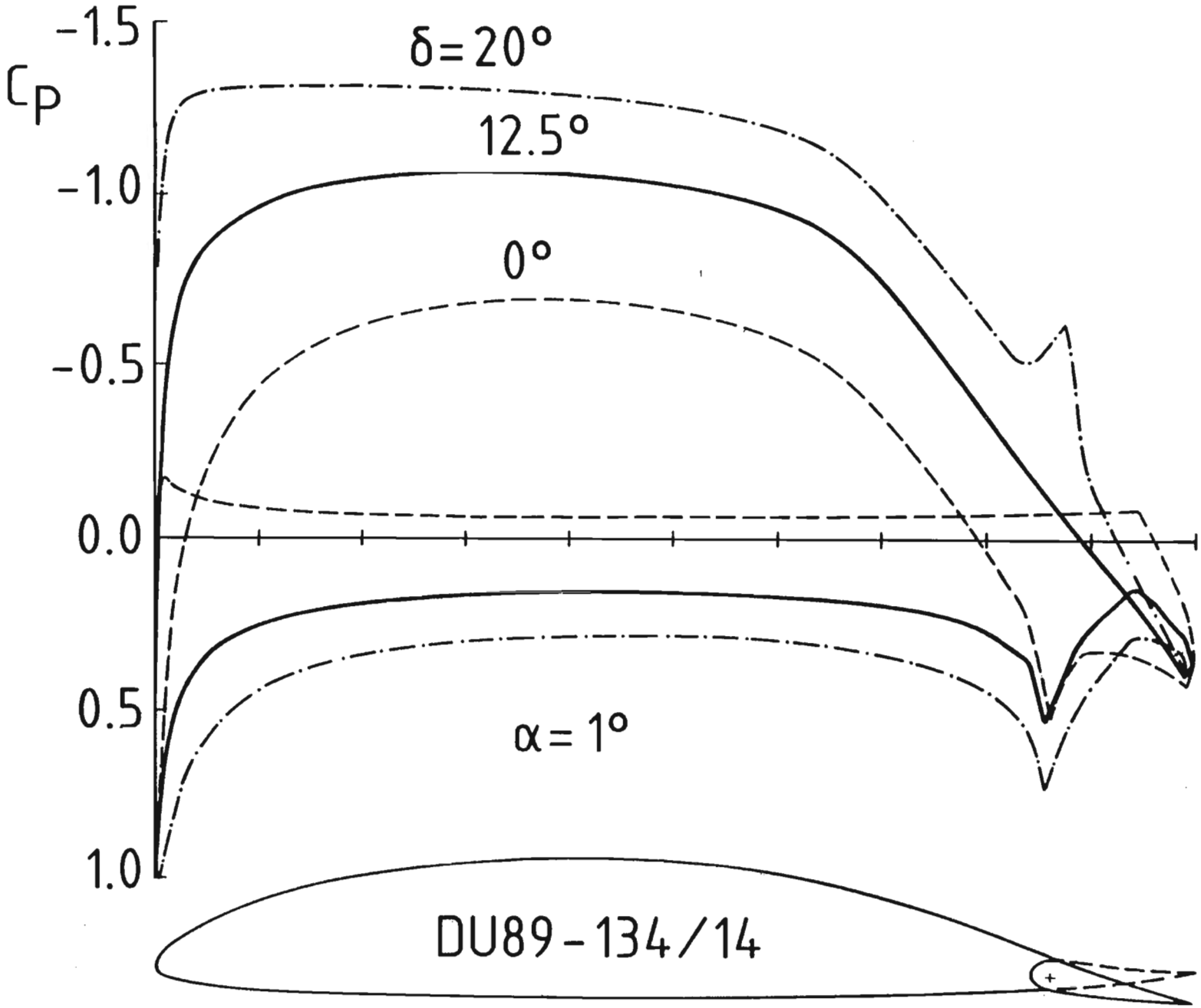
-1.5
C_P
-1.0
-0.5
0.0
0.5
1.0
δ=20°
12.5°
0°
α=1°
DU89-134/14

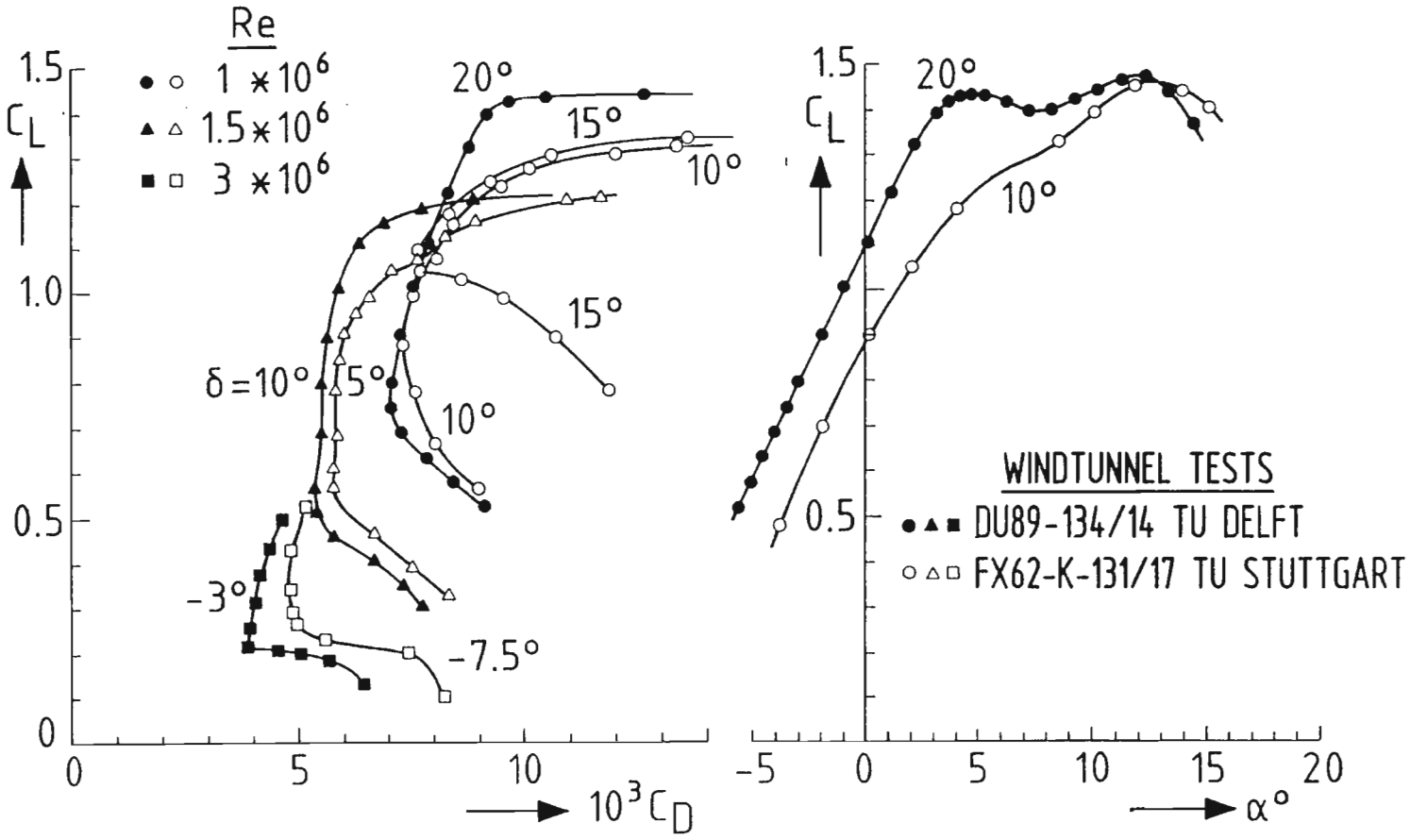
Re
● ○ 1 ∗10⁶
▲ △ 1.5∗10⁶
■ □ 3 ∗10⁶
1.5
C_L
1.0
0.5
0
0
5
10
$10^3 C_D$
20°
15°
10°
15°
δ=10°
5°
10°
-3°
-7.5°
1.5
C_L
20°
10°
0.5
-5
0
5
10
15
20
α°
WINDTUNNEL TESTS
●▲■ DU89-134/14 TU DELFT
○△□ FX62-K-131/17 TU STUTTGART